Earth and Planetary Science Letters 441 (2016) 143–154

Contents lists available at ScienceDirect

Earth and Planetary Science Letters

www.elsevier.com/locate/epsl

The seismic Moho structure of Shatsky Rise oceanic plateau, northwest Pacific Ocean

Jinchang Zhang [a,d,*], William W. Sager [b,d], Jun Korenaga [c]

[a] Key Laboratory of Marginal Sea Geology, South China Sea Institute of Oceanology, Chinese Academy of Sciences, Guangzhou, Guangdong 510301, China
[b] Department of Earth and Atmospheric Sciences, University of Houston, Houston, TX 77204, USA
[c] Department of Geology and Geophysics, Yale University, New Haven, CT 06520, USA
[d] Department of Oceanography, Texas A&M University, College Station, TX 77843, USA

ARTICLE INFO

Article history:
Received 28 November 2015
Received in revised form 21 February 2016
Accepted 23 February 2016
Editor: P. Shearer

Keywords:
oceanic plateau
Shatsky Rise
Moho structure
crustal thickness
reflection and refraction seismics
Airy isostatic compensation

ABSTRACT

Oceanic plateaus are large igneous provinces formed by extraordinary eruptions that create thick oceanic crust, whose structure is poorly known owing to the lack of deep-penetration seismic data. Multichannel seismic (MCS) reflection and wide-angle refraction data allow us to show Moho structure beneath a large part of the Shatsky Rise oceanic plateau in the northwest Pacific Ocean. Moho reflectors in the two data sets can be connected to trace the interface from the adjacent abyssal plain across much of the interior. The reflectors display varied character in continuity, shape, and amplitude, similar to characteristics reported in other locations. Beneath normal crust, the Moho is observed at ~13 km depth (~7 km below the seafloor) in MCS data and disappears at ~20 km depth (~17 km below the seafloor) beneath the high plateau. Moho at the distal flanks dips downward towards the center with slopes of ~0.5°–1°, increasing to 3°–5° at the middle flanks. Seismic Moho topography is consistent with Airy isostasy, confirming this widely-applied assumption. Data from this study show that crustal thickness between the massifs in the interior of the plateau is nearly twice normal crustal thickness, despite the fact that this crust records apparently normal seafloor spreading magnetic lineations. The Moho model allows improved estimates of plateau area (5.33×10^5 km^2) and volume (6.90×10^6 km^3), the latter assuming that the entire crust was formed by Shatsky Rise volcanism because the massifs formed at spreading ridges. This study is unique in showing Moho depth and structure over an extraordinarily large area beneath an oceanic plateau, giving insight to plateau structure and formation.

1. Introduction

The geometry of the Mohorovičić discontinuity (also known as Moho) is important for understanding crustal structure and thickness, the degree and style of isostatic compensation, and magmatic flux from mantle to crust (Steinhart, 1967). The structure of the Moho is still poorly known at most places on Earth because of the scarcity of deep penetration seismic data. Whereas the Moho depth is often inferred by assuming a model of isostatic compensation based on the topography of surface features (e.g., Kearey et al., 2009), seismic measurement is the only direct way to measure Moho structure and assess the validity of isostatic models.

When crustal thickness is on the order of tens of km, our knowledge of the seismic Moho comes primarily from wide-angle seismic refraction (Braile and Chiang, 1986; Mooney and Brocher, 1987). The seismic Moho is defined as a first-order velocity discontinuity where P-wave velocities increase abruptly from crustal values (<7.2 km s^{-1}) to mantle values (>8.0 km s^{-1}) (Rohr et al., 1988; Holbrook et al., 1992). The seismic Moho may not correspond to the petrologic Moho, which is the boundary between non-peridotitic crustal rocks (with gabbroic composition) and olivine-dominated mantle rocks (with peridotitic composition) (Mengel and Kern, 1992; Nedimovic et al., 2005). The advantage of wide-angle refraction for plumbing the Moho is that it can often be inferred from travel time and amplitude differences between the mantle and crustal phases. In some situations, Moho depth can also be estimated directly from seismic waves reflected from the Moho (*PmP* arrivals) (Holbrook et al., 1992). A drawback of this technique is that only a smoothed version of the Moho geometry is inferred from refraction data.

Near-vertical incidence multichannel seismic (MCS) profiling is usually designed to image upper crustal structure, but sometimes reflections from the Moho are observed. MCS data have the advantage of delineating Moho geometry in greater detail than provided by refraction data. Typically the Moho is observed where the crust

* Corresponding author.
E-mail address: jzhang@scsio.ac.cn (J. Zhang).

http://dx.doi.org/10.1016/j.epsl.2016.02.042
0012-821X/

is thin, such as areas of normal oceanic crust (e.g. Kent et al., 1994; Aghaei et al., 2014). In areas with thick crust, such as continental crust, seamounts, and oceanic plateaus, the Moho reflection is suppressed by attenuation unless powerful seismic sources are used. Moho reflections are often intermittent because the near-vertical incidence of seismic waves limits the imaging efficiency at great depths (Mutter and Carton, 2013). Hence, a combination of MCS and wide-angle refraction data can produce a more comprehensive seismic model of the crust than with one method alone (e.g. Mjelde et al., 1993; Gallart et al., 1995; Lizarralde and Holbrook, 1997).

Oceanic plateaus are large submarine mountains, many of which were formed by extensive basaltic volcanism (Coffin and Eldholm, 1994). Wide-angle seismic refraction surveys reveal that they have anomalously thick crust, typically 20–40 km in thickness (Gladczenko et al., 1997; Korenaga, 2011; Charvis and Operto, 1999; Gohl and Uenzelmann-Neben, 2001; Parsiegla et al., 2008; Korenaga and Sager, 2012; Pietsch and Uenzelmann-Neben, 2015). Such thick crust is often compensated nearly completely by Airy isostasy (Sandwell and MacKenzie, 1989). This is because large loads on the lithosphere exceed its yield strength (Watts and Ribe, 1984), particularly when plateaus are formed on the thin lithosphere at or near mid-ocean ridges (Coffin and Eldholm, 1994; Sager, 2005).

Shatsky Rise, located in the northwest Pacific Ocean, ∼1500 km east of Japan, is one of the largest oceanic plateaus. Until recently, its crustal structure was poorly known owing to the lack of modern deep-penetration seismic data. New marine seismic data were recently acquired on two cruises in 2010 and 2012 aboard R/V *Marcus G. Langseth* (MGL1004, MGL1206). During the 2010 cruise, wide-angle seismic refraction data were collected by ocean bottom seismometers (OBS) over the Tamu Massif, the largest edifice within Shatsky Rise (Fig. 1), allowing the construction of a tomographic cross section showing the maximum crustal thickness of ∼30 km (Korenaga and Sager, 2012). On both cruises, two-dimensional MCS reflection profiles were collected over the southern half of Shatsky Rise, giving a detailed picture of the upper crustal structure and showing that Tamu Massif is a massive, single shield volcano with low flank slopes (Sager et al., 2013; Zhang et al., 2015). MCS profiles over Ori Massif, the second largest volcano within Shatsky Rise (Fig. 1), show a similar structure (Zhang et al., 2015). In this paper, we combine MCS and OBS Moho observations from these seismic data to reveal a more complete view of crustal structure beneath the plateau. Shatsky Rise exhibits nearly zero free-air gravity anomaly (Sandwell and Smith, 1997), implying isostatic equilibrium. Thus, the plateau Moho structure is expected to show crustal thickening consistent with the Airy mechanism of isostatic compensation, an assumption that can be tested with the seismic MCS data in this study.

2. Formation and evolution of Shatsky Rise

Shatsky Rise has a reported area of 4.8×10^5 km^2 and consists mainly of three large volcanic highs, Tamu, Ori, and Shirshov massifs, and a low ridge, Papanin Ridge, extending from its north side (Fig. 1; Sager et al., 1999). Elevations are 3–4 km above the surrounding seafloor, which lies at ∼6–5.5 km water depth. The shallowest point is ∼1950 m water depth at the summit of Toronto Ridge, a late stage eruptive feature that rises from the top of Tamu Massif (Sager et al., 1999).

Because it is situated exactly at the junction of two Mesozoic magnetic lineation sets, the Japanese and Hawaiian lineations (Larson and Chase, 1972), Shatsky Rise must have erupted at a triple junction, likely with a ridge-ridge-ridge geometry (Hilde et al., 1976; Sager et al., 1988; Nakanishi et al., 1999). Initial Shatsky Rise eruptions began with Tamu Massif, which was emplaced just after the time of adjacent magnetic chron M21 (Nakanishi et al., 2015) (149 Ma, here and elsewhere using the time scale of Gradstein et al. (2012) for magnetic lineation ages), which is consistent with radiometric dates of 144.6 ± 0.8 Ma (Mahoney et al., 2005) and 144.4 ± 1.0 Ma (Heaton and Koppers, 2014) from basalt cores recovered, respectively, at Ocean Drilling Program (ODP) Site 1213 on the south flank of Tamu Massif and Integrated Ocean Drilling Program (IODP) Site U1347 on the east flank (Fig. 1). Toronto Ridge is ∼15 Myr younger than the Tamu Massif shield (Heaton and Koppers, 2014) and other similar ridges and parasitic cones occur on the Shatsky Rise massifs (Sager et al., 1999), implying post-shield building volcanism, but it appears that this late-stage volcanism was small in volume and did not greatly postdate the main edifice. Thus, the crustal structure of Shatsky Rise probably did not change appreciably after the primary eruptions.

Magnetic anomalies show that the age of the seafloor becomes younger to the NE and the axis of Shatsky Rise coincides with the triple junction until chron M1 (126 Ma) (Fig. 1). This age progression implies that Ori and Shirshov massifs and Papanin Ridge were emplaced progressively along the triple junction path after it moved NE away from Tamu Massif (Sager et al., 1999; Nakanishi et al., 1999). Tamu Massif may have formed rapidly, within a period of 3–4 million years or less (Sager and Han, 1993; Heaton and Koppers, 2014); however, based on the span of magnetic anomalies, it took ∼23 million years for the entire ∼2000 km length of Shatsky Rise to form.

Shatsky Rise is mostly covered by thin pelagic sediments of ≤∼300 m (Ludwig and Houtz, 1979), except for thick sediment accumulations up to ∼1 km thickness that are limited to the summits of the massifs (Sliter and Brown, 1993; Sager et al., 1999). Basaltic lava flow samples were recovered from Shatsky Rise at ODP Site 1213 (Shipboard Scientific Party, 2001; Koppers et al., 2010) and at IODP sites U1346, U1347, U1349 and U1350 (Sager et al., 2010, 2011), confirming the volcanic nature of this oceanic plateau.

3. Data and methods

Prior to the two recent seismic cruises, no digital, deep penetration seismic data had been collected over Shatsky Rise. Two OBS refraction lines (Korenaga and Sager, 2012) were obtained over Tamu Massif and twelve MCS reflection profiles, totaling 3350 km in length (Zhang et al., 2015), were recorded over the southern half of Shatsky Rise (Fig. 1). Both refraction and reflection data were acquired using a source array with 36-airguns (volume 108.2 L), but with 162-m and 50-m shot spacing, respectively. The refraction data were analyzed by joint reflection and refraction travel time tomography, defining crustal structure beneath center of Tamu Massif (Korenaga and Sager, 2012). For the reflection study, a 6-km-long, 468-channel streamer (hydrophone array) with a 12.5-m group interval was used as the receiver. The streamer and airgun array were towed in 9 m depth beneath the sea surface, with a 172-m offset from the source to the first channel. The raw data had a primary energy frequency range of 2–206 Hz. The reflection data were processed into time sections with common MCS processing steps, resolving the upper crustal structure to depths of 1–4 km (Sager et al., 2013; Zhang et al., 2015). All digitized interfaces (seafloor, igneous basement and the Moho) were picked in phase with the maximum positive amplitude of the reflection.

Although a Moho reflector was commonly observed in the MCS profiles with standard processing, these data were reprocessed using constant velocity stacks (CVS) to enhance these reflections. CVS is a processing method that uses a constant velocity for the entire time domain to stack the CMP traces, whereas normal CMP stacking uses a depth-dependent velocity model from semblance

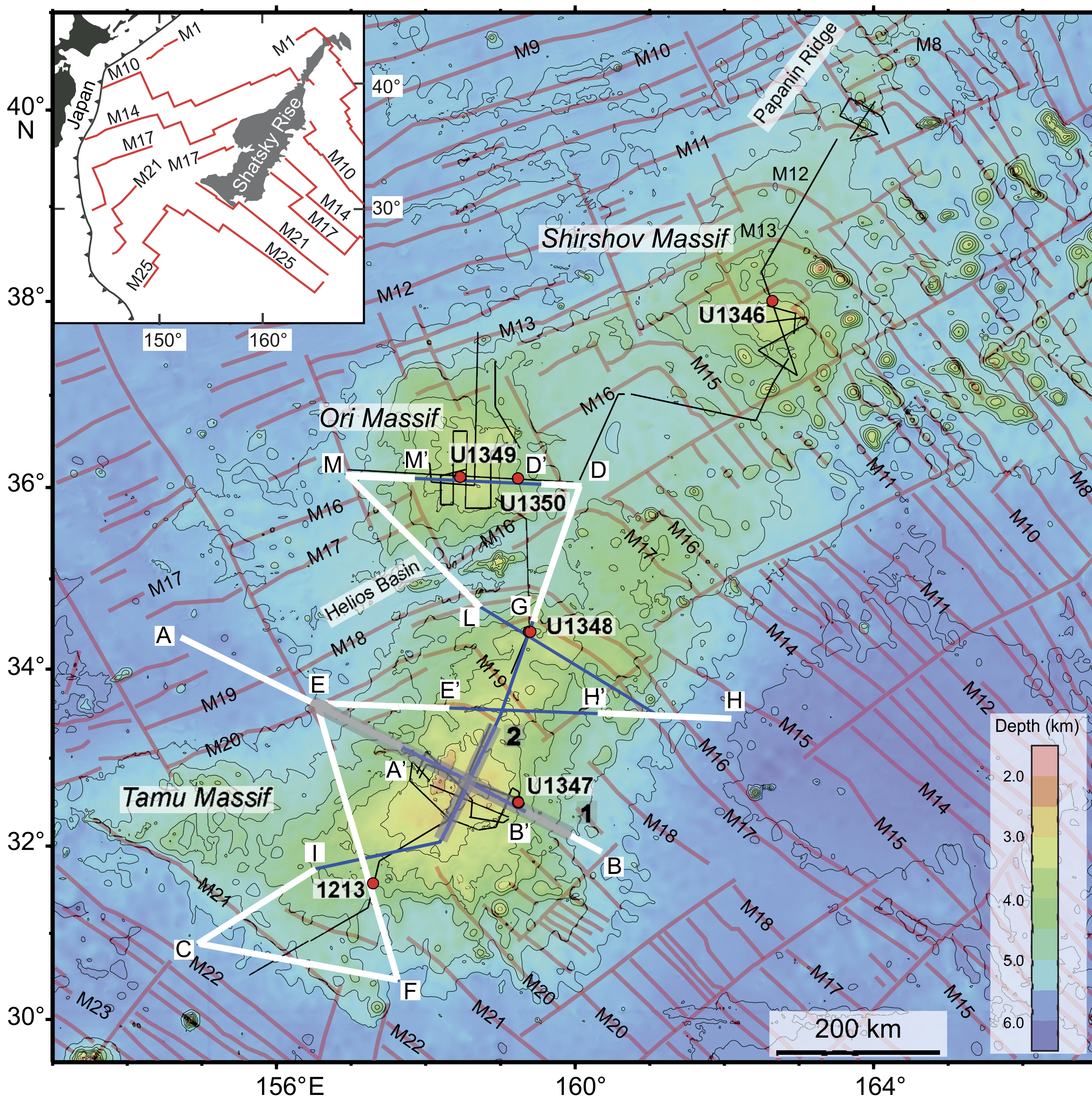

Fig. 1. Bathymetry and tectonic map of Shatsky Rise with seismic track lines. Bathymetry is from satellite-predicted depths with 500-m contours (Smith and Sandwell, 1997). Heavy red lines show magnetic lineations with chron numbers labeled for reference (Nakanishi et al., 1999). Heavy blue lines show MCS reflection profiles collected by R/V *Marcus G. Langseth* on cruises MGL1004 and MGL1206. White lines denote seismic sections that display the Moho reflection, whereas blue lines are those that do not. Letters identify sections discussed in the text. Heavy gray lines with numbers 1 and 2 are OBS refraction lines (Korenaga and Sager, 2012). Thin black lines show seismic reflection profiles collected during cruise TN037 (Klaus and Sager, 2002). Filled red circles show locations of ODP and IODP drill sites mentioned in the text. Inset depicts the location of Shatsky Rise relative to Japan and nearby subduction zones (toothed lines) and the wider magnetic pattern. (For interpretation of the references to color in this figure legend, the reader is referred to the web version of this article.)

velocity analysis. Because the Moho reflection is deep, weak in amplitude, and intermittent, it is difficult to obtain an optimal stacking velocity for the Moho by examining the semblance. What is more, velocities within the thick crust cannot be analyzed by this method because no coherent reflectors are observed in the middle and lower crust. CVS thus has the advantage of simplicity, but it also improved the visibility of the Moho reflector in seismic sections. We tested a range of plausible velocities (3000–5000 $\mathrm{m\,s^{-1}}$ with a 100 $\mathrm{m\,s^{-1}}$ step length) for CVS stacking to find the value that provided the clearest image (4000 $\mathrm{m\,s^{-1}}$). CVS can highlight the reflectivity of a particular horizon, at the expense of degrading the image quality of structures above, which may not be properly stacked by CVS. As a result, CVS cannot be used as standard seismic reflection imaging for a complete section. For imaging the deep, isolated Moho reflectors, however, this approach is simple and practical.

The Moho was interpreted as the deepest visible reflector in MCS reflection profiles. It typically appears as the only coherent reflection in a section otherwise devoid of such signals. Although there is no independent verification that this reflector is the Moho, there is no other plausible interpretation for the reflection at the observed travel-times. Furthermore, interpretation of this reflection as Moho is consistent with OBS refraction data as described below.

To compare results from OBS refraction and MCS reflection data and to generate composite crustal structure sections, refraction Moho depths were taken from the seismic tomography model of Korenaga and Sager (2012), whereas MCS reflection Moho depths were calculated from reflector two-way travel time with assumed

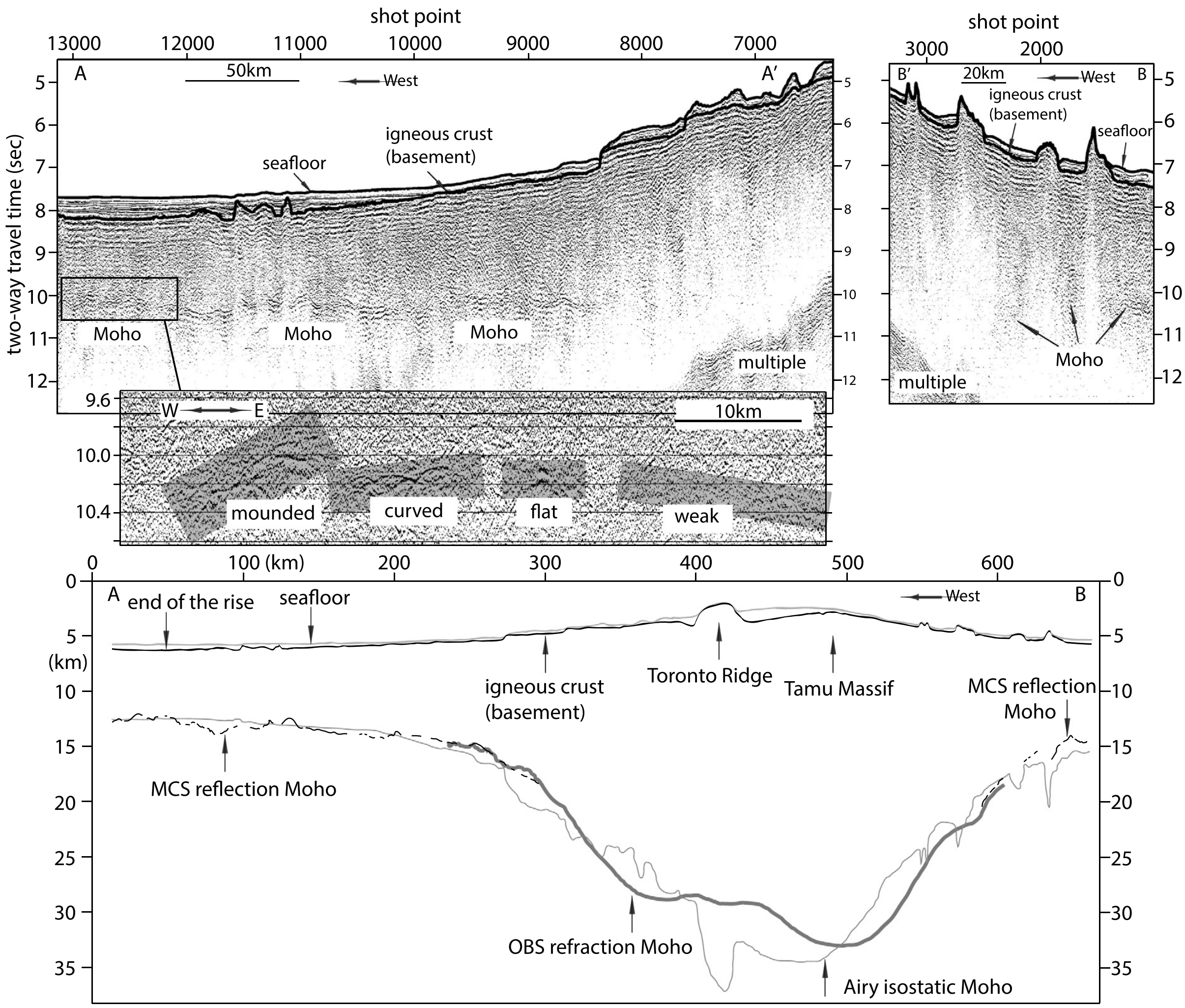

Fig. 2. MCS reflection images and crustal structure of line A–B, across the center of Tamu Massif. Top panel shows MCS reflection images for the line segments A–A′ and B–B′, which display Moho reflectors. Boxed area is enlarged to show Moho reflector detail. Bottom panel shows the interpretation of crustal structure along line A–B. The light gray and black lines represent the seafloor and top of igneous crust, respectively. The intermittent heavy black lines show the MCS reflection Moho. The heavy dark gray line shows the Moho traced by OBS refraction data (Korenaga and Sager, 2012). The light gray line shows the predicted Moho from Airy isostasy. Vertical exaggeration = 7:1. Locations shown in Fig. 1.

velocities for the water column, sediment and igneous crust of 1500 m s^{-1}, 2000 m s^{-1} and 6575 m s^{-1}, respectively. The latter value has the greatest effect on calculated MCS Moho depth. It was determined by minimizing the RMS misfit between observed (OBS) and calculated (MCS) Moho depths; the minimum RMS misfit is 0.48 km, and the 2σ (∼95%) confidence limits on the average crustal velocity are estimated as ±439 m s^{-1}. In addition, this average crustal velocity matches well with the velocity-depth profile from Korenaga and Sager (2012). For MCS reflection sections in the absence of refraction data (lines E–H, E–F, C–F, M–D, M–L, Fig. 1) or where the refraction data and reflection data do not overlap (line C–D, Fig. 1), the same velocities were used to calculate Moho depths from two-way travel time.

In order to compare Shatsky Rise Moho structure to Airy isostatic compensation, the expected Airy Moho depth (assuming 100% compensation) was calculated from the observed depth of the igneous basement. Knowing h, the height above the abyssal plain depth, the thickness of the crustal root, r, was calculated as: $r = h(\rho_c - \rho_w)/(\rho_m - \rho_c)$, where ρ_c is the average density of oceanic crust, ρ_w is water density, and ρ_m is mantle density. Reference values for determining h and r were determined from the observed average basement depth (5.8 km) and average Moho depth (12.8 km) in the adjacent abyssal plain west of Tamu Massif. The density contrast ratio $(\rho_c - \rho_w)/(\rho_m - \rho_c)$ is the multiplier that converts height h to root thickness r. We used a ratio of 6.15 to calculate Airy Moho depths, which was determined by minimizing the average misfit where the Airy-calculated and seismic-observed Moho depths overlapped in all seismic lines (Figs. 2–8). The minimum RMS misfit is 2.33 km, with the 95% confidence limits on the density contrast ratio of ±1.64. Using the water density of 1000 kg m^{-3} and the mantle density of 3300 kg m^{-3}, the ratio of 6.15 implies the crustal density of 2980 kg m^{-3}. Using the empirical density–velocity relation of Carlson and Herrick (1990), this crustal density would correspond to the P-wave velocity of ∼7.3 km s^{-1}, considerably higher than the aforementioned average crustal velocity of ∼6.6 km s^{-1}. There are at least two possible explanations for this discrepancy. First, the average density is a simple arithmetic mean, but the average velocity is a harmonic mean, so it is biased to the lower-velocity upper crustal section. Second, the empirical relation of Carlson and Herrick (1990) is based on laboratory measurements of samples collected from the oceanic crust and ophiolites, so it may not be applicable to thick oceanic plateaus. These possibilities can be quantified by a joint consideration of seismic data and gravity (e.g., Korenaga et al., 2001), and it will be explored elsewhere.

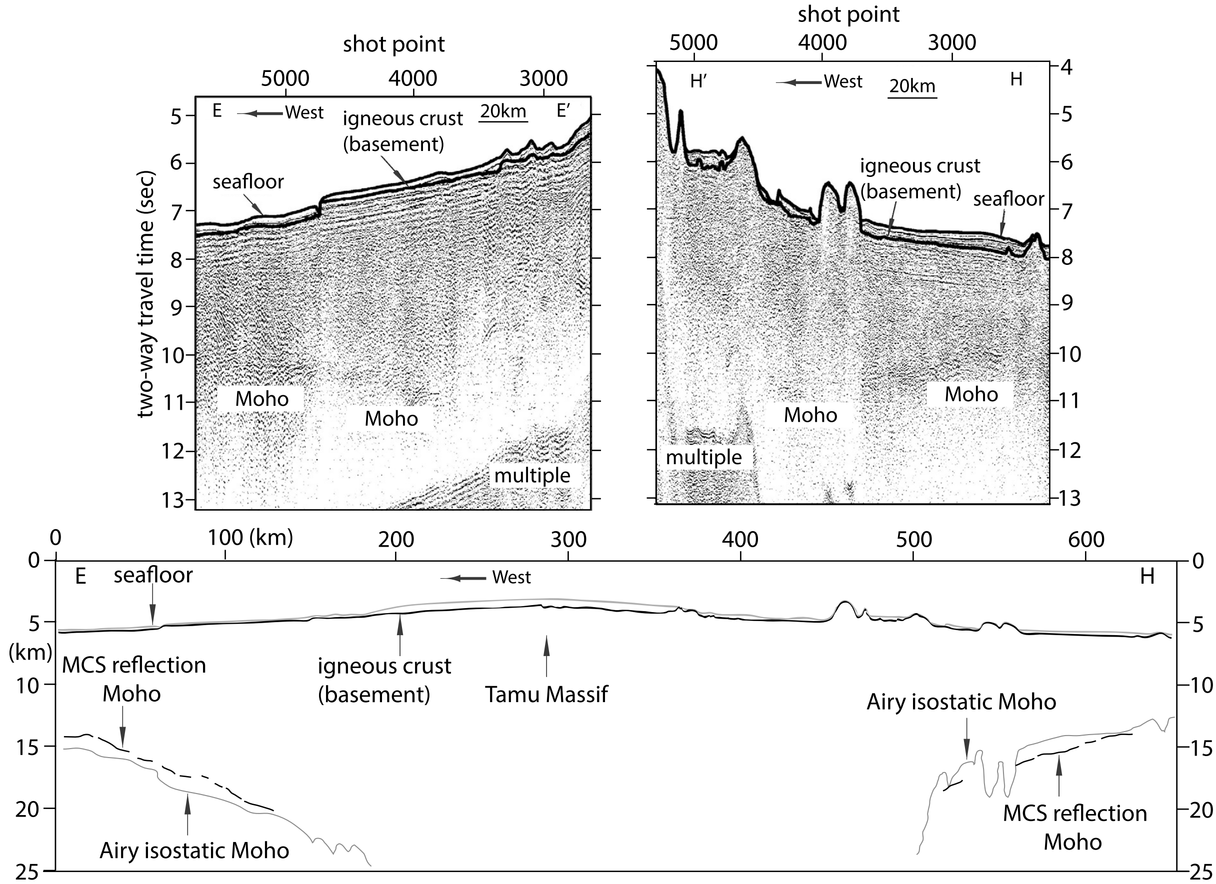

Fig. 3. MCS reflection images and crustal structure of line E–H, on the north side of Tamu Massif. Top panel shows MCS reflection images for line segments E–E′ and H–H′, which display the Moho reflection. Bottom panel shows crustal structure of line E–H. Locations shown in Fig. 1. Other plot conventions as in Fig. 2.

To determine the crustal thickness distribution of Shatsky Rise, we need to estimate Moho depths and exclude the sediments atop igneous basement. For Moho depths, we used our seismic Moho observations along the reflection and refraction profiles shown in this paper. Where Moho was not observed seismically, we calculated Airy isostatic model-predicted Moho depths based on satellite-predicted bathymetry (Smith and Sandwell, 1997). To exclude sediments, there are other seismic lines available in regions of the massif summits where sediments are thick (Zhang et al., 2015), so it was possible to determine the igneous basement depth and to use this horizon as the top of the calculated volume. For other areas where sediments are thin and seismic data are few or unavailable, we used an average sediment thickness of 300 m to estimate the depth of the basement.

Given the crustal thickness distribution of Shatsky Rise, we can calculate the area and the igneous crustal volume of Shatsky Rise. We created a 1-min-spacing grid of longitude and latitude ranging from 152° to 170° E and 29° to 45° N, respectively, which contains the entire rise. In this Moho grid, we assumed that the plateau crust was inside the contiguous area where the crust exceeds a thickness of 7 km. At each grid node, the basement depth and sediment thickness were used to calculate Moho depth based on the aforementioned formula.

4. Results

4.1. Reflection Moho characteristics

Reflection Moho is frequently observed on MCS profiles over Shatsky Rise, but it is not observed everywhere. Specifically, the MCS line segments containing the Moho reflection are located on the lower flanks of the massif and on the surrounding seafloor (Fig. 1). In the summit areas, where the crust is thickest (Korenaga and Sager, 2012), Moho reflections are not observed.

Moho reflectors are highly variable in (Figs. 2–8): (1) segment length, ranging from several to tens of kilometers; (2) shape, ranging from flat to curved or mounded; and (3) strength, ranging from sharp and high amplitude to weak or absent. In general, the Moho reflectors are discontinuous, with gaps of a few kilometers between segments, becoming weaker approaching the center of the massifs. However, adjacent individual reflectors can be connected by following their trend to infer the large-scale structure of the Moho.

4.2. Seismic Moho under Shatsky Rise

4.2.1. Tamu Massif

At Tamu Massif, discontinuous Moho reflectors are observed beneath the lower flanks, starting from a depth of ∼10 s two-way travel time (TWTT) (∼13 km), and dipping towards the middle of the massif with shallow slopes of ∼0.5°–1° beneath the distal flanks. At a distance of ∼150 km from the center, the dip increases to ∼3°–5° before flattening beneath the center of the massif. The Moho disappears at a depth of ∼11 s TWTT (∼20 km), where multiples occur (lines A–B, E–H, E–F, C–F and C–D, Figs. 2–6). In the seismic time sections, the Moho appears nearly flat (e.g., Fig. 2), within a narrow range of travel times (10–11 s TWTT) because of velocity pull-up in the rising volcanic mountain.

When the surface topography is rough due to the occurrence of secondary cones (Zhang et al., 2015), the Moho usually disappears (e.g. SP 1500, 2000 on line A–B, Fig. 2; SP 3800 and 4600 on line

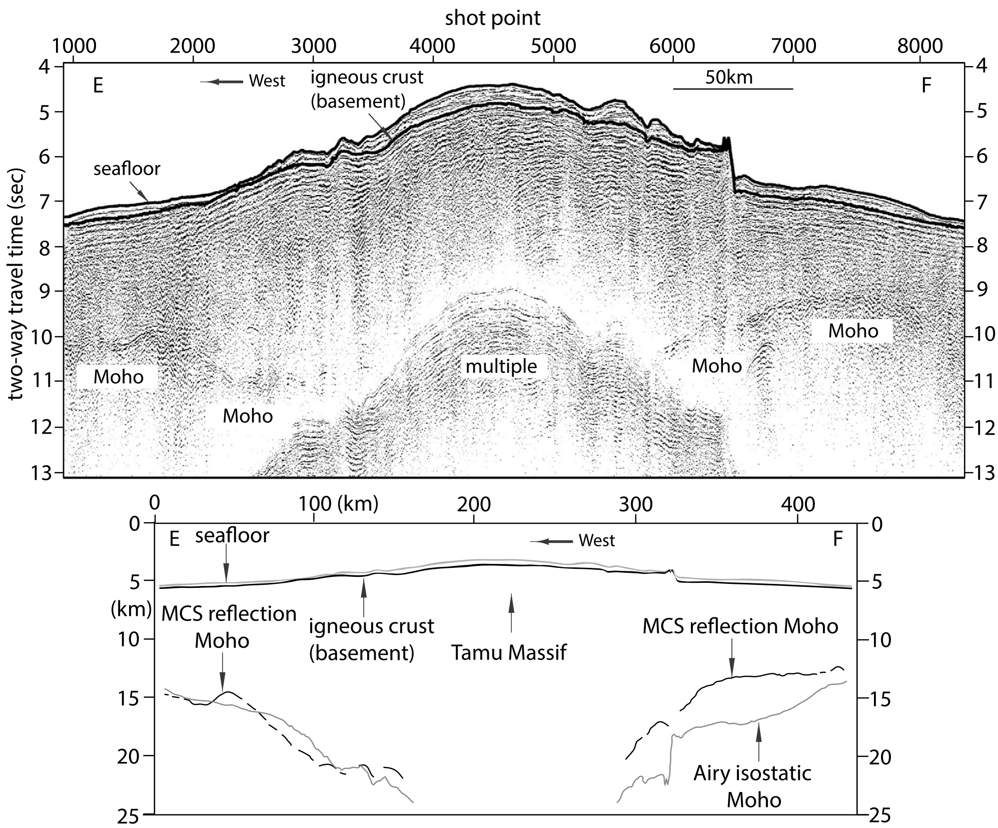

Fig. 4. MCS reflection image and crustal structure of line E–F, on the south flank of Tamu Massif. Top panel shows MCS reflection image. Bottom panel shows crustal structure. Location shown in Fig. 1. Other plot conventions as in Fig. 2.

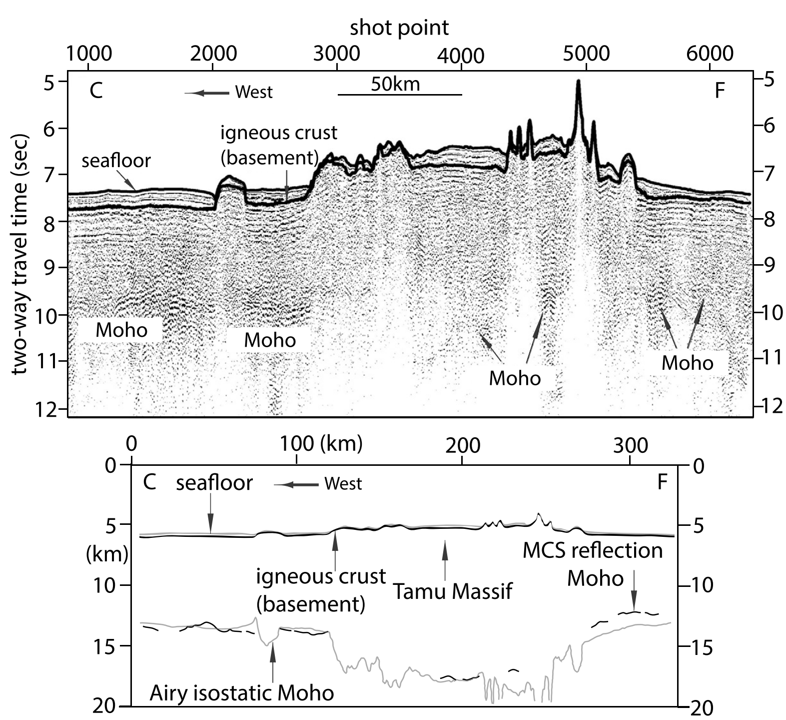

Fig. 5. MCS reflection image and crustal structure of line C–F, on the distal south flank of Tamu Massif. Top panel is MCS reflection image. Bottom panel shows crustal structure. Location shown in Fig. 1. Other plot conventions as in Fig. 2.

E–H, Fig. 3; SP 6500 on line E–F, Fig. 4; SP 2000, 3000, 5000 on line C–F, Fig. 5; SP 1500, 3200 on line C–D, Fig. 6), probably because the surface cones scatter or attenuate the seismic signal.

MCS reflection images do not show the Moho near the center of Tamu Massif. Fortunately, two refraction lines (lines 1, 2; Fig. 1) cross the center of this mountain and show the Moho struc-

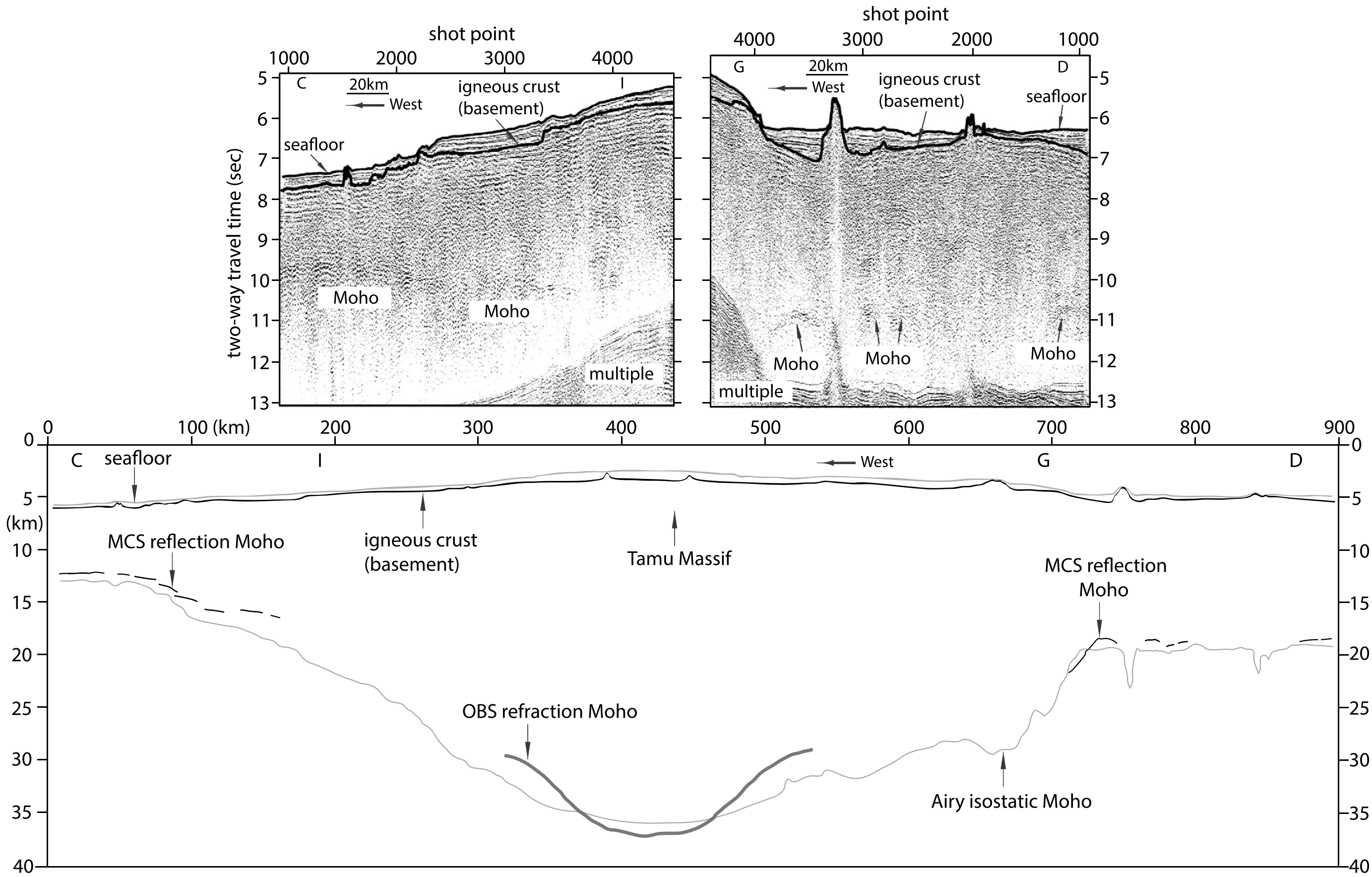

Fig. 6. MCS reflection images and crustal structure of line C–D, along the axis of Tamu Massif. Top panel shows MCS reflection images of segments C–I and G–D, which display the Moho reflection. Segment C–I is located on the south flank, whereas segment G–D is located on the north flank. Bottom panel shows crustal structure of line C–D. Letters at top refer to segment endpoints. Locations shown in Fig. 1. Other plot conventions as in Fig. 2.

ture beneath the thickest part of the massif (Korenaga and Sager, 2012). The MCS data are complementary and can be combined to generate a complete composite Moho profile across the massive structure (Figs. 2, 6).

The maximum crustal thickness (∼30 km) occurs beneath the buried shield summit (Korenaga and Sager, 2012; Sager et al., 2013) on Line A–B at 490 km (Fig. 2). Although Toronto Ridge (at 410 km) is the shallowest basement peak, it does not correspond to the thickest part of the crust, consistent with the interpretation that this ridge is a late-stage feature and the shield summit was the center of shield-building volcanism (Sager et al., 2013; Zhang et al., 2015) and is thus supported mostly by lithospheric strength.

A similar crustal structure is observed on Line C–D, a ∼900 km profile along the SW–NE axis of Tamu Massif, perpendicular to Line A–B (Figs. 1, 6). The seismic Moho on this profile is not as complete as that on Line A–B because the refraction profile is short (Korenaga and Sager, 2012). The refraction Moho shows a narrower root than on Line A–B, but this may be an artifact of the short length of the refraction profile. In addition, the northeast end of Line C–D, which is within the interior of Shatsky Rise, shows a crustal thickness of ∼13 km.

4.2.2. Ori Massif

Beneath Ori Massif, like Tamu Massif, the Moho reflection is observed at the lower flanks (Line M–D, Fig. 1). On this profile, two profile segments (M–M′ and D–D′, Fig. 7) on the western and eastern ends of Ori Massif show a few weak Moho reflectors that dip ∼5° towards the center of the Massif and disappear around the time of the multiples. The continuity of the Moho appears different on either side with Moho beneath segment M–M′ being more continuous than that beneath segment D–D′. Owing to the short length of the seismic profile, no observations of Moho were gathered in the abyssal plains adjacent to Ori Massif (Fig. 7). At the ends of this profile, the crustal thickness is ∼12–13 km.

Line M–L, which crosses the southwestern flank of Ori Massif and the Helios Basin, between Ori and Tamu massifs, displays Moho reflectors on both ends of the line (Fig. 8). At the western end of line M–L, the Moho declines ∼3° towards the center of Ori Massif, reaching a depth of ∼11.3 s TWTT (∼22.5 km) before fading around the multiples. Unlike Fig. 7, the mirror Moho reflection in Fig. 8 is poorly observed on the east side of Ori Massif, even though the surface topography is smoother than the west side and less scattering would be expected. Additionally, a strong Moho reflector dips ∼5° away from Ori Massif beneath Helios Basin, the basin separating Ori Massif from the north flank of Tamu Massif (Fig. 8). This reflector dips towards the center of Tamu Massif, so it is likely part of the root of that feature. Interestingly, the observed Moho depth implies thickened crust (∼12 km) beneath this basin, so it is not floored by normal ocean crust, despite the occurrence of seafloor spreading magnetic anomalies within (Nakanishi et al., 1999).

4.3. Airy isostatic Moho

Although the Airy isostatic Moho was calculated using a simple model of oceanic crust with constant densities (i.e., no horizontal density contrasts), it matches well with the seismic reflection and refraction Mohoin most places (Figs. 2–8), with a RMS misfit of 2.33 km. This broad agreement shows that the observed seis-

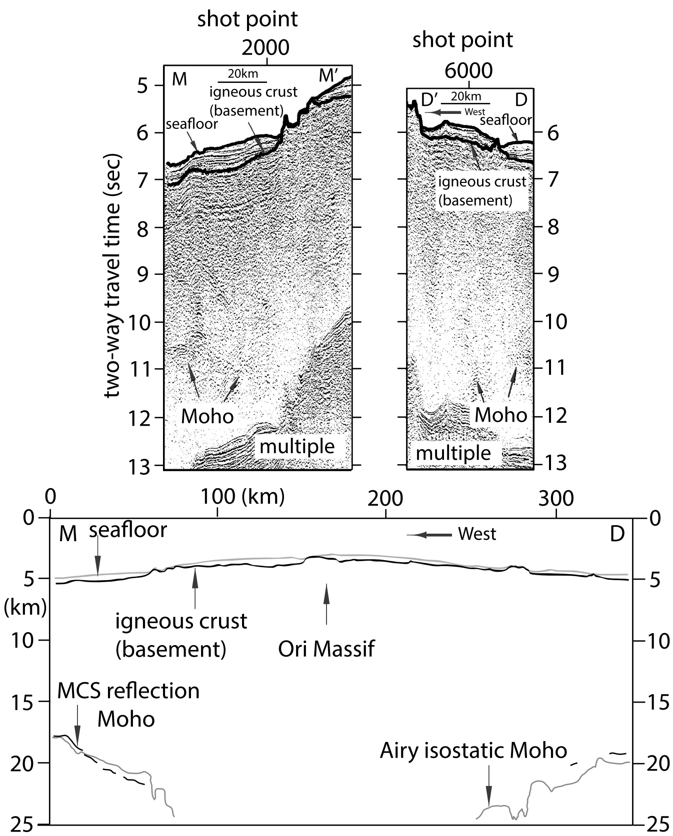

Fig. 7. MCS reflection images and crustal structure of line M–D, across Ori Massif. Top panel shows MCS reflection images of segments M–M′ and D–D′, which display the Moho reflection. Bottom panel shows crustal structure of line M–D. Locations shown in Fig. 1. Other plot conventions as in Fig. 2.

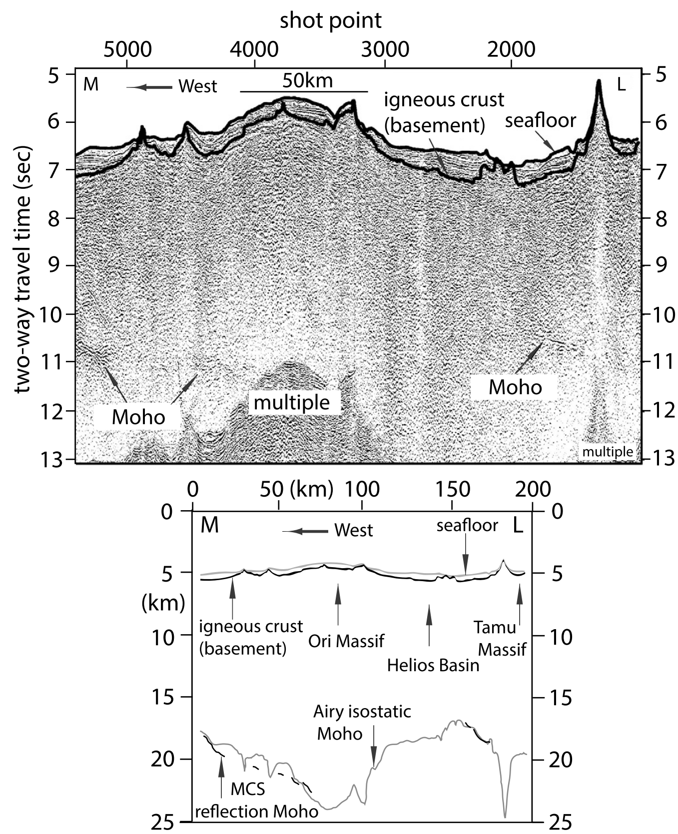

Fig. 8. MCS reflection images and crustal structure of line M–L, on the southwest flank of Ori Massif and across Helios Basin. Top panel shows MCS reflection image. Bottom panel shows crustal structure. Location shown in Fig. 1. Other plot conventions as in Fig. 2.

mic and inferred Moho locations support the idea that the depth of this horizon is determined by Airy isostasy. Two notable exceptions are the summit of Tamu Massif along line A–B (Fig. 2) and the eastern half of line E–F (Fig. 4). The line A–B mismatch probably occurs because of the difference between primary crustal construction and later modifications. Toronto Ridge (at 410 km in Fig. 2) is a secondary volcanic feature (Sager et al., 1999, 2013; Heaton and Koppers, 2014; Zhang et al., 2015) that is probably supported mostly by crustal strength, rather than root buoyancy. It causes an overestimation of root depth underneath because the root is calculated based on the Airy assumption that the root reflects surface topography. In addition, the thick sediment pond (maximum ∼1 km thickness) located between ∼430 and 480 km, causes an overestimation of root depth by implying thicker crust. Another mismatch occurs on the southern half of line E–F (Fig. 4). The calculated Airy isostatic Moho fits the reflection Moho on the western side but not the eastern side, where the calculated Airy Moho is 2–2.5 km too deep, implying anomalously higher mantle–crust density contrast ratio. The discrepancy implies something must be different on the eastern side of the line from the western side. A similar discrepancy with smaller amplitude is also seen at the end of line C–F (Fig. 5), and one possible explanation is that there exists some extra buoyancy, other than the crustal component, around the waypoint F. This waypoint corresponds to the beginning of Shatsky Rise formation, so melt migration might have been inefficient, resulting in frozen gabbroic veins within the shallow mantle. Another possibility is that what is identified as the MCS reflection Moho on the east half of the line C–F is actually the base of the pre-existing crust, and there may be crustal underplating beneath it because there seems to be sub-Moho reflectivity at SP 6750 (Fig. 4).

4.4. The area and volume of Shatsky Rise

Because the observed Moho fits the Airy calculation well in most places, we used this assumption to calculate predicted Moho depths and crustal thickness across the Shatsky Rise environs (Fig. 9). The crustal thickness can be used to estimate the lateral boundary of Shatsky Rise, which is necessary to determine the area and volume of the plateau. The western part of line A–B (Fig. 2) extends into the normal abyssal basin, where the acoustic basement and Moho appear flat, indicating the crust beyond Shatsky Rise. This occurs at around SP 12600 and corresponds to a crustal thickness of ∼7 km. By using this 7-km thickness as the boundary of the rise (the outer edge of the colored area in Fig. 9), the area of Shatsky Rise was calculated to be 5.33×10^5 km^2. Excluding sediment cover (see Data and Methods section), the total volume estimate of Shatsky Rise crust is 6.90×10^6 km^3.

5. Discussion

5.1. Moho reflectors

In the MCS reflection data presented here, the Moho reflectors are observed on the lower flanks of Tamu Massif and on the surrounding seafloor, whereas the Moho reflectors are not observed beneath the central parts of the massifs, where the crust is thickest (Korenaga and Sager, 2012). There is a tendency for the Moho to be more continuous and clearly observed on the periphery of Shatsky Rise, as compared with the lower flanks of massifs in the interior. The absence of Moho reflections beneath the centers of the massifs may result from two factors. One explanation is that strong multiples mask the Moho reflectors in these areas (e.g. Figs. 2, 4).

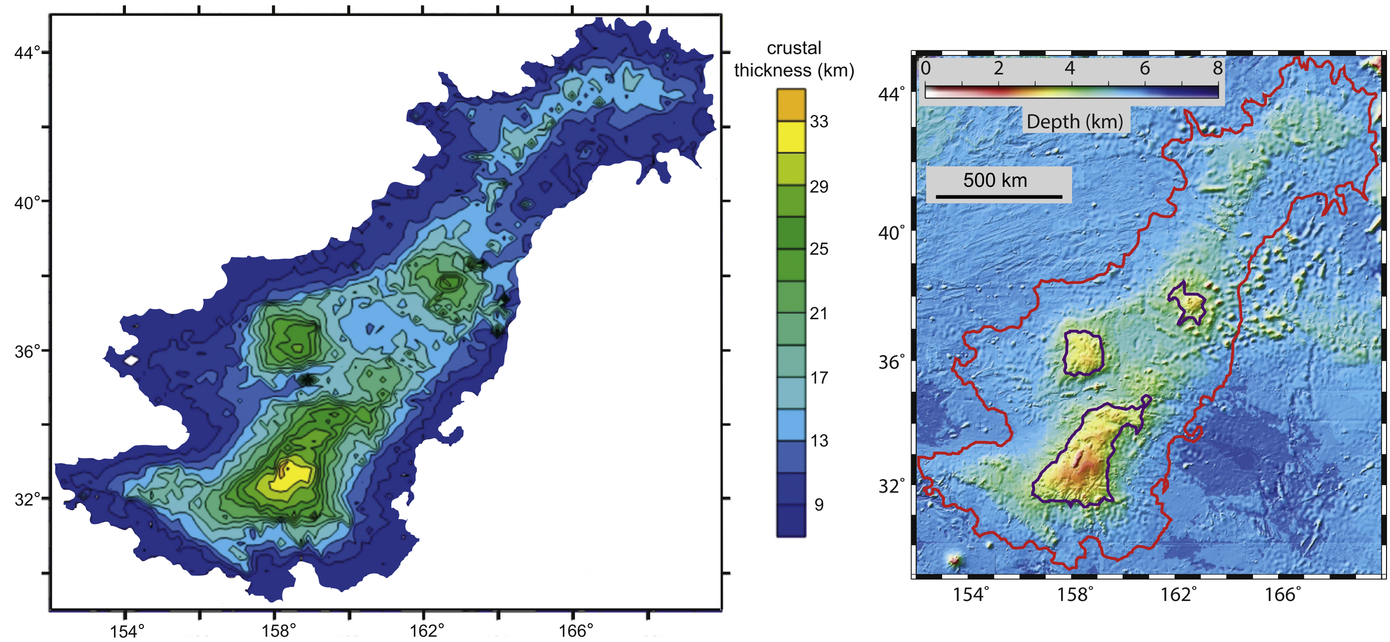

Fig. 9. Left panel is spatial extent and crustal thickness distribution of Shatsky Rise, determined from MCS Moho observations and Airy isostasy model (where Moho was not observed). Spatial extent of Shatsky Rise is outlined at 7 km crustal thickness. Thickness contour interval is 2 km. Right panel is bathymetry map of Shatsky Rise with crustal thickness contours. Bathymetry is from satellite-predicted depths with 500-m contours (Smith and Sandwell, 1997). Red and purple lines show 7-km and 21-km Moho contours, respectively. (For interpretation of the references to color in this figure legend, the reader is referred to the web version of this article.)

Another is that the seismic signal is attenuated with greater depth in the crust and the return is too weak to be observed.

MCS reflection data in this study show Moho reflectors that are highly variable in length (continuity), morphology, and strength (amplitude). This variability is similar to that observed both at mid-ocean ridges and over normal oceanic crust (Kent et al., 1994; Mutter and Carton, 2013; Aghaei et al., 2014). Two explanations for Moho variability are suggested by Mutter and Carton (2013). One is that the real Moho structure varies from an abrupt vertical discontinuity to a broad gradient zone. The other explanation is that scattering in the crust results in variable imaging conditions at the Moho level, so that the variability is apparent and does not correspond to structural complexity of the Moho. In the Shatsky Rise MCS reflection profiles, we often observe that the Moho is absent beneath secondary cones or large faults (e.g. Fig. 5). Where the upper crustal topography is smooth, we often observe continuous Moho reflectors. This correspondence suggests that Moho reflections are affected by near-surface structure. Although this relationship is generally true for Shatsky Rise MCS data, there are exceptions. For instance, at SP 1100 of Fig. 5, the upper crustal topography is horizontally layered, but no Moho reflectors are observed. Scattering within the upper oceanic crust, therefore, cannot completely explain the absence of the Moho reflector. In the lower crust, the rough topography of Moho itself may also scatter acoustic energy, i.e., a Moho that is structurally complex may not give coherent reflection, resulting in an incoherent Moho reflector, as was observed on Juan de Fuca ridge flanks (Nedimovic et al., 2005).

5.2. *Moho structure below Shatsky Rise*

As observed on Shatsky Rise MCS reflection lines, the Moho bounds a deep crustal root. Line A–B (Fig. 2) is a remarkable profile across the center of Tamu Massif showing a complete profile of Moho structure from combined MCS reflection and refraction data. It is unique to show Moho depth and structure over an extraordinarily large area beneath a large oceanic plateau, because other large oceanic plateaus are lack of comparable MCS studies, which only discuss shallow structures like sediments and igneous basement. The Moho is horizontal beneath the abyssal plain ocean crust, but shows a slight dip at the edges of the massif towards the massif center. At mid-massif flanks, Moho dip increases before flattening again beneath the plateau center. Interestingly, the zones of steeper Moho occur beneath prominent escarpments, which are thought to represent down-to-basin normal faults (Zhang et al., 2015), suggesting a possible connection. The faults have been explained by differential subsidence of the plateau center and flanks, with the center sinking less owing to underplating (Ito and Clift, 1998). Perhaps the rapid increase in crustal thickness causes the lower flanks and mid-flanks to experience different subsidence rates. At odds with this interpretation, the refraction velocity profile (Korenaga and Sager, 2012) shows no high velocity zone in the lower crust beneath the massif summit that would imply underplating, instead, high velocity zones occur near the zones of steeper Moho dip (Korenaga and Sager, 2012), suggesting it is the flanks that are anomalous.

The crustal structure of Shatsky Rise is consistent with Airy isostasy. This observation confirms inferences from gravity data, which show small free air anomalies over Shatsky Rise (and other oceanic plateaus) (Sandwell and Mackenzie, 1989). Although this result was expected from gravity studies, the MCS data directly confirm the Airy model, which is based on crustal and mantle density assumptions that are rarely tested by direct observation. Shatsky Rise was built on young oceanic lithosphere with little rigidity, so the plateau formed in isostatic equilibrium with a deep crustal root.

Moho data show that the crust within the interior of Shatsky Rise between Tamu and Ori massifs is unusually thick. Our Moho reflections on lines G–D and L–M (Figs. 6, 8) show a thickness almost twice that of normal oceanic crust thickness ($\sim$13 km vs. $\sim$7 km) in these locations. This thick crust has clearly been affected by excess volcanism. This is an important observation because previous studies have shown that these areas contain identifiable magnetic anomalies recorded by seafloor spreading (Nakanishi et al., 1999; Sager et al., 1988, 1999). These authors speculated that the crust between massifs is essentially normal and much of the plateau height in the interior may be ponded sediments. Our data imply that the crust is significantly thicker than normal. Weakening this interpretation is the fact that we only have two lines that image the plateau interior between massifs. Nevertheless, there is no reason to think the locations between Ori and Tamu massifs are different from other locations within the plateau.

5.3. Area and volume of Shatsky Rise

Prior estimates of the area and volume of Shatsky Rise were simplistic, using a particular bathymetry contour to define the edge of the plateau and the Airy isostasy assumption to calculate crustal thickness. Using a bathymetry contour to delineate the edge is problematic because deeper contours around Shatsky Rise are not closed, so it is necessary to extrapolate where depth contours depart from the shape of the plateau. A better estimate can be made using crustal thickness, derived from Airy calculations. Moreover, with the new seismic data as confirmation for crustal thickness, area and volume estimates can be more reliable.

Sliter and Brown (1993) estimated the area of Shatsky Rise above the 5000-m bathymetry contour as 7.50×10^5 km^2, whereas Sager et al. (1999) calculated an area of 4.80×10^5 km^2 using the same contour. The reason for the great difference is unclear because both estimates are not documented well. Our estimate of 5.33×10^5 km^2 is more accurate because it uses a crustal thickness to define the model edge, rather than extrapolated depth contours.

For an indication of the precision of our estimate of the edge of Shatsky Rise, using 7 km thickness, we note that increasing the threshold crustal thickness to 7.5 km (an increase of 7%) results in a ∼8% decrease of area and ∼5% of volume. Thus, the estimate of area and volume is not greatly affected by our choice of the threshold thickness.

Calculating the crustal volume of Shatsky Rise, it is necessary to make an assumption about pre-existing crust. One approach is to assume that the volcanic structures were emplaced atop normal oceanic crust (e.g., Sager et al., 1999). This method is appropriate for intraplate volcanoes. An alternative method is to assume that the volcanic edifices were formed by volcanism at the ridge crest, forming thickened oceanic crust. For the former, we subtract the 7 km thickness of the normal oceanic crust from the total volume, but for the latter, the entire volume of the crust is assumed to be part of Shatsky Rise. Using the entire crust, the total volume is 6.90×10^6 km^3, but excluding 7-km-thick pre-existing crust, the volume is reduced to 3.17×10^6 km^3. The latter figure can be considered the "excess" magmatic emplacement and corresponds to the estimate given by Sager et al. (1999). Recent dating of basaltic rock samples cored from Sites 1213 and U1347 give ages that are close to that the underlying magnetic lineations (Mahoney et al., 2005; Heaton and Koppers, 2014). It is thus clear that the Shatsky Rise edifices formed very close to the spreading ridge crest. Given that the magma sources for both volcanoes (Shatsky Rise and the mid-ocean ridge) were so close that they probably cannot have been distinguished, the distinction between Shatsky Rise volcanoes and the oceanic crust may be inappropriate, and the larger volume estimate is more appropriate.

The calculated volume of Shatsky Rise can be used to estimate the volume of source mantle for the Shatsky Rise volcanism. Husen et al. (2013) estimated 20–23% of partial melting for rocks cored from Shatsky Rise. Assuming 20% partial melting, the volume of the source mantle must have been 3.5×10^7 km^3, which corresponds to a sphere with a radius of ∼200 km.

6. Conclusions

MCS reflection data show extensive Moho reflectors beneath Shatsky Rise oceanic plateau. The Moho reflectors are highly variable in: (1) length, ranging from several to tens of kilometers; (2) shape, ranging from flat to curved or mounded; and (3) strength, ranging from sharp and strong to weak or absent, similar to Moho observations in other settings. Moho reflectors are discontinuous, but individual reflectors can be connected into long, piecewise-continuous horizons by tracing along their trend. The Moho reflectors are observed mainly beneath the lower flanks of the oceanic plateau; those closer to the center of the massifs are weaker, and the Moho reflection is absent beneath the thickest crust, probably because of greater attenuation with depth and masking by multiples.

The Moho reflectors are shallow (∼7 km) beneath normal crust near the distal flanks of Shatsky Rise massifs and dip downward towards the center of the massif from all directions. The dip is slight beneath the distal flanks (0.5°–1°) but increases to 3°–5° beneath the middle flanks. Moho depths from MCS reflection data can be matched with those from refraction data beneath Tamu Massif, providing a complete Moho profile across the massif with a maximum thickness of ∼30 km at the center. Moho profiles show that crust between Tamu and Ori massifs, within the interior of Shatsky Rise, is almost twice as thick as normal oceanic crust, indicating excess volcanism despite the recording of coherent magnetic lineations by this crust.

The Shatsky Rise Moho geometry is consistent with nearly complete Airy isostasy. Although this result was expected from gravity studies, the MCS data directly confirm the Airy model, which is based on assumptions about crustal and mantle density. Shatsky Rise was built on young oceanic lithosphere with little rigidity, so the plateau formed in isostatic equilibrium with a deep crustal root.

Based on observed and calculated Moho, including the rise with crustal thickness over 7 km, the spatial extent of Shatsky Rise was estimated with a total area of 5.33×10^5 km^2 and a total volume of 6.90×10^6 km^3. The latter estimate assumes that the entire crust was formed by Shatsky Rise volcanism because the massifs formed at spreading ridges.

Acknowledgements

We would like to thank the captain, crew, and technical staff of the R/V *Marcus G. Langseth* for assisting in collection of geophysical data during two cruises. We are indebted to Seismic Micro Technology, Inc. and Halliburton, Inc. for making seismic analysis software available at no cost or reduced cost. This project was supported by National Science Foundation grants OCE-0926945 and OCE-0926611, National Natural Science Foundation of China grants 91328205 and 41376062, Key Laboratory of Marine Mineral Resources, Ministry of Land and Resources of China grant KLMMR-2014-B-06, Key Laboratory of Marginal Sea Geology, Chinese Academy of Sciences grant MSGL15-04, Natural Science Foundation of Guangdong Province in China grant 2015A030310374, Ministry of Human Resources and Social Security of China grant 50603-54, the Mariana Trench Project of the South China Sea Institute of Oceanology of Chinese Academy of Sciences, and China Scholarship Council for joint education program between Texas A&M University and Ocean University of China. We thank two anonymous reviewers for helpful critique.

References

Aghaei, O., Nedimovic, M.R., Carton, H., Carbotte, S.M., Canales, J.P., Mutter, J.C., 2014. Crustal thickness and Moho character of the fast-spreading East Pacific Rise from 9°42′N to 9°57′N from poststack-migrated 3D MCS data. Geochem. Geophys. Geosyst. 15 (3), 634–657. http://dx.doi.org/10.1002/2013GC005069.

Braile, L.W., Chiang, C.S., 1986. The continental Mohorovičić discontinuity: results from near-vertical and wide-angle seismic refraction studies. In: Barazangi, M., Brown, L. (Eds.), Reflection Seismology: A Global Perspective. In: American Geophysical Union Geodynamics Series, vol. 13. Washington, DC, pp. 257–272.

Carlson, R.L., Herrick, C.N., 1990. Densities and porosities in the oceanic crust and their variations with depth and age. J. Geophys. Res. 95 (B6), 9153–9170. http://dx.doi.org/10.1029/JB095iB06p09153.

Charvis, P., Operto, S., 1999. Structure of the Cretaceous Kerguelen Volcanic Province (southern Indian Ocean) from wide-angle seismic data. J. Geodyn. 28 (1), 51–71. http://dx.doi.org/10.1016/S0264-3707(98)00029-5.

Coffin, M.F., Eldholm, O., 1994. Large igneous provinces: crustal structure, dimensions, and external consequences. Rev. Geophys. 32 (1), 1–36. http://dx.doi.org/10.1029/93RG02508.

Gallart, J., Vidal, N., Danobeitia, J.J., 1995. Multichannel seismic image of the crustal thinning at the NE Iberian margin combining normal and wide angle reflection data. Geophys. Res. Lett. 22 (22), 489–492. http://dx.doi.org/10.1029/94GL03272.

Gladczenko, T.P., Coffin, M.F., Eldholm, O., 1997. Crustal structure of the Ontong Java Plateau: modeling of new gravity and existing seismic data. J. Geophys. Res. 102 (102), 22711–22729. http://dx.doi.org/10.1029/97JB01636.

Gohl, K., Uenzelmann-Neben, G., 2001. The crustal role of the Agulhas Plateau, southwest Indian Ocean: evidence from seismic profiling. Geophys. J. Int. 144 (3), 632–646. http://dx.doi.org/10.1046/j.1365-246x.2001.01368.x.

Gradstein, F.M., Ogg, J.G., Smith, A.G., 2012. The Geologic Time Scale. Cambridge University Press, Cambridge.

Heaton, D.E., Koppers, A.A., 2014. Constraining the rapid construction of Tamu Massif at a ∼145 Myr old triple junction, Shatsky Rise. In: Goldschmidt Conference. Sacramento, abstract 948.

Hilde, T.W., Isezaki, C.N., Wageman, J.M., 1976. Mesozoic seafloor spreading in the north central Pacific. In: Sutton, G.H., Manghnani, M.H., Moberly, R., McAfee, E.U. (Eds.), The Geophysics of the Pacific Ocean Basin and Its Margin. In: American Geophysical Union Geophysical Monograph Series, vol. 19. Washington, DC, pp. 205–226.

Holbrook, W.S., Reiter, E.C., Purday, G.M., Toksoz, M.N., 1992. Image of the Moho across the continent–ocean transition, United States east-coast. Geology 20 (3), 203–206. http://dx.doi.org/10.1130/0091-7613(1992)020<0203:IOTMAT>2.3.CO;2.

Husen, A., Almeev, R.R., Holtz, F., Koepke, J., Sano, T., Mengel, K., 2013. Geothermobarometry of basaltic glasses from the Tamu Massif, Shatsky Rise oceanic plateau. Geochem. Geophys. Geosyst. 14 (10), 3908–3928. http://dx.doi.org/10.1002/ggge.20231.

Ito, G., Clift, P.D., 1998. Subsidence and growth of Pacific Cretaceous plateaus. Earth Planet. Sci. Lett. 161 (1), 85–100. http://dx.doi.org/10.1016/S0012-821X(98)00139-3.

Kearey, P., Klepeis, K.A., Vine, F.J., 2009. Global Tectonics, third edition. Wiley–Blackwell, United Kingdom.

Kent, G.M., Harding, A.J., Orcutt, J.A., Detrick, R.S., Mutter, J.C., Buhl, P., 1994. Uniform accretion of oceanic crust south of the Garrett transform at 14°42′S on the East Pacific Rise. J. Geophys. Res. 99 (B5), 9097–9116. http://dx.doi.org/10.1029/93JB02872.

Klaus, A., Sager, W.W., 2002. Data report: high-resolution site survey seismic reflection data for ODP Leg 198 drilling on Shatsky Rise, northwest Pacific. In: Bralower, T.J., Premoli Silva, I., Malone, M.J., et al. (Eds.), Proceedings of the Ocean Drilling Program, Initial Reports, vol. 198. Ocean Drilling Program, College Station, pp. 1–21.

Koppers, A.A.P., Sano, T., Natland, J.H., Widdowson, M., Almeev, R., Greene, A.R., Murphy, D.T., Delacour, A., Miyoshi, M., Shimizu, K., Li, S., Hirono, N., Geldmacher, J., the Expedition 324 Scientists, 2010. Massive basalt flows on the southern flank of Tamu Massif, Shatsky Rise: a reappraisal of ODP Site 1213 basement units. In: Sager, W.W., Sano, T., Geldmacher, J., the Expedition 324 Scientists (Eds.), Proceedings of the Integrated Ocean Drilling Program, vol. 324. Integrated Ocean Drilling Program Management International, Inc., Tokyo, pp. 1–20.

Korenaga, J., Holbrook, W.S., Detrick, R.S., Kelemen, P.B., 2001. Gravity anomalies and crustal structure across the southeast Greenland margin. J. Geophys. Res. 106 (B6), 8853–8870. http://dx.doi.org/10.1029/2000JB900416.

Korenaga, J., 2011. Velocity-depth ambiguity and the seismic structure of large igneous provinces: a case study from the Ontong Java Plateau. Geophys. J. Int. 185 (2), 1022–1036. http://dx.doi.org/10.1111/j.1365-246X.2011.04999.x.

Korenaga, J., Sager, W.W., 2012. Seismic tomography of Shatsky Rise by adaptive importance sampling. J. Geophys. Res. 117 (B8), 70–83. http://dx.doi.org/10.1029/2012JB009248.

Larson, R.L., Chase, C.G., 1972. Late Mesozoic evolution of the western Pacific Ocean. Geol. Soc. Am. Bull. 83 (12), 3627–3644. http://dx.doi.org/10.1130/0016-7606(1972)83[3627:LMEOTW]2.0.CO;2.

Lizarralde, D., Holbrook, W.S., 1997. U.S. Mid-Atlantic margin structure and early thermal evolution. J. Geophys. Res. 102 (B10), 22855–22875. http://dx.doi.org/10.1029/96JB03805.

Ludwig, W.J., Houtz, R.E., 1979. Isopach Map of Sediments in the Pacific Ocean Basin and Marginal Sea Basins. American Association of Petrolem Geologists, Tulsa, Oklahoma.

Mahoney, J.J., Duncan, R.A., Tejada, M.L.G., Sager, W.W., Bralower, T.J., 2005. Jurassic–Cretaceous boundary age and mid-ocean ridge type mantle source for Shatsky Rise. Geology 33 (3), 185–188. http://dx.doi.org/10.1130/G21378.1.

Mengel, K., Kern, H., 1992. Evolution of the petrological and seismic Moho-implications for the continental crust–mantle boundary. Terra Nova 4 (4), 109–116. http://dx.doi.org/10.1111/j.1365-3121.1992.tb00455.x.

Mjelde, R., Sellevoll, M.A., Shimamura, H., Iwasaki, T., Kanazawa, T., 1993. Crustal structure beneath Lofoten, N. Norway, from vertical incidence and wide-angle seismic data. Geophys. J. Int. 114 (1), 116–126. http://dx.doi.org/10.1111/j.1365-246X.1993.tb01471.x.

Mooney, W.D., Brocher, T.M., 1987. Coincident seismic reflection/refraction studies of the continental lithosphere: a global review. Rev. Geophys. 25 (4), 723–742. http://dx.doi.org/10.1029/RG025i004p00723.

Mutter, J.C., Carton, H.D., 2013. The Mohorovicic discontinuity in ocean basins: some observations from seismic data. Tectonophysics 609 (1), 314–330. http://dx.doi.org/10.1016/j.tecto.2013.02.018.

Nakanishi, M., Sager, W.W., Klaus, A., 1999. Magnetic lineations within Shatsky Rise, northwest Pacific Ocean: implications for hot spot-triple junction interaction and oceanic plateau formation. J. Geophys. Res. 104 (B4), 7539–7556. http://dx.doi.org/10.1029/1999JB900002.

Nakanishi, M., Sager, W.W., Korenaga, J., 2015. Reorganization of the Pacific–Izanagi–Farallon triple junction in the Late Jurassic: tectonic events before the formation of the Shatsky Rise. In: Neal, C.R., Sager, W.W., Sano, T., Erba, E. (Eds.), The Origin, Evolution, and Environmental Impact of Oceanic Large Igneous Provinces. In: Geophysical Society of America Special Paper, vol. 511. Boulder, pp. 85–102.

Nedimovic, M.R., Carbotte, S.M., Harding, A.J., Detrick, R.S., Canales, J.P., Diebold, J.B., Kent, G.M., Tischer, M., Babcock, J.M., 2005. Frozen magma lenses below the oceanic crust. Nature 436 (7054), 1149–1152. http://dx.doi.org/10.1038/nature03944.

Parsiegla, N.K., Gohl, K., Uenzelmann-Neben, G., 2008. The Agulhas Plateau: structure and evolution of a large igneous province. Geophys. J. Int. 174 (1), 336–350. http://dx.doi.org/10.1111/j.1365-246X.2008.03808.x.

Pietsch, R., Uenzelmann-Neben, G., 2015. The Manihiki Plateau – a multistage volcanic emplacement history. Geochem. Geophys. Geosyst. 16 (8), 2480–2498. http://dx.doi.org/10.1002/2015GC005852.

Rohr, K.M.M., Milkereit, B., Yorath, C.J., 1988. Asymmetric deep crustal structure across the Juan de Fuca Ridge. Geology 16 (6), 533–537. http://dx.doi.org/10.1130/0091-7613(1988)016<0533:ADCSAT>2.3.CO;2.

Sager, W.W., 2005. What built Shatsky Rise, a mantle plume or ridge tectonics? In: Foulger, G.R., Natland, J.H., Presnall, D.C., Anderson, D.L. (Eds.), Plates, Plumes, and Paradigms. In: Geophysical Society of America Special Paper, vol. 388. Boulder, pp. 721–733.

Sager, W.W., Han, H.C., 1993. Rapid formation of the Shatsky Rise oceanic plateau inferred from its magnetic anomaly. Nature 364 (6438), 610–613. http://dx.doi.org/10.1038/364610a0.

Sager, W.W., Handschumacher, D.W., Hilde, T.W.C., Bracey, D.R., 1988. Tectonic evolution of the northern Pacific plate and Pacific–Farallon–Izanagi triple junction in the Late Jurassic and Early Cretaceous (M21–M10). Tectonophysics 155 (1–4), 345–364. http://dx.doi.org/10.1016/0040-1951(88)90274-0.

Sager, W.W., Kim, J., Klaus, A., Nakanishi, M., Khankishieva, L.M., 1999. Bathymetry of Shatsky Rise, northwest Pacific Ocean: implications for ocean plateau development at a triple junction. J. Geophys. Res. 104 (B4), 7557–7576. http://dx.doi.org/10.1029/1998JB900009.

Sager, W.W., Sano, T., Geldmacher, J., the Expedition 324 Scientists, 2010. Proceedings of the Integrated Ocean Drilling Program, vol. 324. Integrated Ocean Drilling Program Management International, Inc., Tokyo.

Sager, W.W., Sano, T., Geldmacher, J., 2011. How do oceanic plateaus form? Clues from drilling at Shatsky Rise. Eos Trans. AGU 92 (5), 37–44. http://dx.doi.org/10.1029/2011EO050001.

Sager, W.W., Zhang, J., Korenaga, J., Sano, T., Koppers, A.A.P., Mahoney, J., Widdowson, M., 2013. An immense shield volcano within the Shatsky Rise oceanic plateau, northwest Pacific Ocean. Nat. Geosci. 6 (11), 976–981. http://dx.doi.org/10.1038/ngeo1934.

Sandwell, D.T., MacKenzie, K.R., 1989. Geoid height versus topography for oceanic plateaus and swells. J. Geophys. Res. 94 (B6), 7403–7418. http://dx.doi.org/10.1029/JB094iB06p07403.

Sandwell, D.T., Smith, W.H.F., 1997. Marine gravity anomaly from Geosat and ERS-1 satellite altimetry. J. Geophys. Res. 102 (B5), 10039–10054. http://dx.doi.org/10.1029/96JB03223.

Shipboard Scientific Party, 2001. Leg 192 summary. In: Mahoney, J.J., Fitton, J.G., Wallace, P.J., Coffin, M. (Eds.), Proceedings of the Ocean Drilling Program, Initial Reports, vol. 192. Ocean Drilling Program, College Station.

Sliter, W.V., Brown, G.R., 1993. Shatsky Rise: seismic stratigraphy and sedimentary record of Pacific paleoceanography since the Early Cretaceous. In: Natland, J.H., Storms, M.A., et al. (Eds.), Proceedings of the Ocean Drilling Program, Scientific Results, vol. 132. Ocean Drilling Program, College Station.

Smith, W.H.F., Sandwell, D.T., 1997. Global seafloor topography from satellite altimetry and ship depth soundings. Science 277 (5334), 1957–1962. http://dx.doi.org/10.1126/science.277.5334.1956.

Steinhart, J.S., 1967. Mohorovicic discontinuity. In: Runcorn, S.K. (Ed.), International Dictionary of Geophysics, vol. 2. Pergamon Press, Oxford, pp. 991–994.

Watts, A.B., Ribe, N.M., 1984. On geoid heights and flexure of the lithosphere at seamounts. J. Geophys. Res. 89 (B13), 11152–11170. http://dx.doi.org/10.1029/JB089iB13p11152.

Zhang, J., Sager, W.W., Korenaga, J., 2015. The Shatsky Rise oceanic plateau structure from two-dimensional multichannel seismic reflection profiles and implications for oceanic plateau formation. In: Neal, C.R., Sager, W.W., Sano, T., Erba, E. (Eds.), The Origin, Evolution, and Environmental Impact of Oceanic Large Igneous Provinces. In: Geophysical Society of America Special Paper, vol. 511. Boulder, pp. 103–126.